JOURNAL OF CHEMICAL INFORMATION AND MODELING

ARTICLE

pubs.acs.org/jcim

Solvated Interaction Energy (SIE) for Scoring Protein−Ligand Binding Affinities. 2. Benchmark in the CSAR-2010 Scoring Exercise

Traian Sulea,*[,†] Qizhi Cui,[†] and Enrico O. Purisima[†]

[†]Biotechnology Research Institute, National Research Council Canada, 6100 Royalmount Avenue, Montreal, Quebec H4P 2R2, Canada

Supporting Information

ABSTRACT: Solvated interaction energy (SIE) is an end-point physics-based scoring function for predicting binding affinities from force-field nonbonded interaction terms, continuum solvation, and configurational entropy linear compensation. We tested the SIE function in the Community Structure−Activity Resource (CSAR) scoring challenge consisting of high-resolution cocrystal structures for 343 protein−ligand complexes with high-quality binding affinity data and high diversity with respect to protein targets. Particular emphasis was placed on the sensitivity of SIE predictions to the assignment of protonation and tautomeric states in the complex and the treatment of metal ions near the protein−ligand interface. These were manually curated from an originally distributed CSAR-HiQ data set version, leading to the currently distributed CSAR-NRC-HiQ version. We found that this manual curation was a critical step for accurately testing the performance of the SIE function. The standard SIE parametrization, previously calibrated on an independent data set, predicted absolute binding affinities with a mean-unsigned-error (MUE) of 2.41 kcal/mol for the CSAR-HiQ version, which improved to 1.98 kcal/mol for the upgraded CSAR-NRC-HiQ version. Half−half retraining-testing of SIE parameters on two predefined subsets of CSAR-NRC-HiQ led to only marginal further improvements to an MUE of 1.83 kcal/mol. Hence, we do not recommend altering the current default parameters of SIE at this time. For a sample of SIE outliers, additional calculations by molecular dynamics-based SIE averaging with or without incorporation of ligand strain, by MM-PB(GB)/SA methods with or without entropic estimates, or even by the linear interaction energy (LIE) formalism with an explicit solvent model, did not further improve predictions.

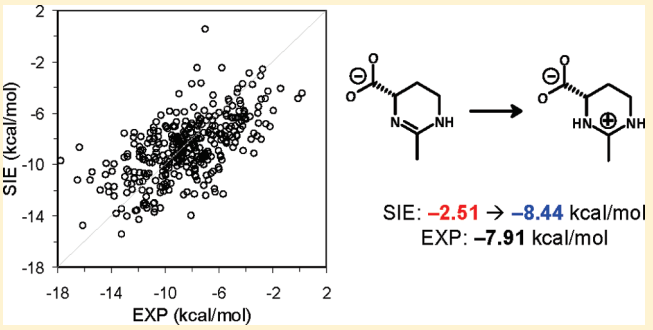

INTRODUCTION

Accurate prediction of protein−ligand binding affinities is critical for successful structure-based drug design and for understanding the thermodynamic aspects of molecular recognition in biological systems. A large and ever-increasing number of binding affinity prediction methods emerged over the past few years in order to address the "scoring problem".[1−3] Current scoring functions can be classified into three main categories: empirical, knowledge-based, and force field−based.[4]

The solvated interaction energy (SIE) method belongs to the group of end-point force field−based scoring functions that represent a reasonable compromise between time, computational resources, and accuracy. SIE approximates the protein−ligand binding free energy in aqueous solution by an interaction energy contribution and a desolvation free energy contribution, each of them further made up of an electrostatic component and a nonpolar component.[5,6] This approximation to binding free energy in solution resembles the formalism used in other physics-based binding free energy end-point calculation methods, including MM-PB(GB)/SA and linear interaction energy (LIE).[7−11]

Estimation of binding affinities within this formalism is dependent on several physical properties of the system, such as the solute internal dielectric constant, atomic Born radii, atomic partial charges, and nonpolar surface tension coefficient. There is considerable uncertainty about the exact values for some of these physical properties in various systems. For example, solute dielectric values adopted by practitioners for electrostatic calculations in protein−ligand systems range between 1 and 20, which leads to dramatically varied results. While the huge effect of different values for solute dielectric can be effectively offset by appropriate scaling of atomic Born radii for electrostatic solvation calculations, such a buffering effect is lost for electrostatic binding calculations. This suggested the calibration of optimal values for physical parameters directly against binding data.[12]

Hence, the physical parameter space of the SIE function was previously explored on a protein−ligand data set consisting of 99 complexes with known binding affinities and cocrystal structures solved at high-resolution.[5] Because the objective was to calibrate a generic SIE function applicable to a broad range of protein−ligand systems, the assembled SIE training data set included

Special Issue: CSAR 2010 Scoring Exercise

Received: January 18, 2011
Published: June 29, 2011

11 diverse protein targets each with a short congeneric series of ligands, with binding affinities curated from the literature spanning 14 kcal/mol. A training performance characterized by 1.34 kcal/mol mean-unsigned-error (MUE) and 1.76 kcal/mol root-mean-square-error (RMSE), with Pearson squared correlation coefficient (R^2) of 0.65 and Spearman-rho rank correlation coefficient (ρ_S) of 0.79 can be achieved with a SIE functional form that retains the physical meaning and interpretability of the optimal parameters (Figure S1A). Particularly, optimal solute dielectric falls within the range of 2 to 4 in agreement with refractive index measurements of protein powders, and there is a scaling down of the potential energy plus solvation by about 90% likely reflecting the compensation exerted by the configurational entropy loss arising form narrowing of the energy wells in the complex versus the free state.[13,14]

There are two main application modes of the SIE function. The first application mode, employed during SIE calibration, is based on an energy-minimized single-conformation structure of the complex — for example a cocrystal structure or a ligand computationally docked to the protein.[5] The second application mode, called *sietraj*, is based on a molecular dynamics (MD) trajectory and is similar in spirit to the single-trajectory MM-PB(GB)/SA approach.[6,7] In both modes, rigid infinite separation of the complex into protein and ligand to generate the free state is applied, with replacement of the explicit solvent by a continuum model. Practical notes for carrying out SIE calculations have been written.[15]

Several tests and applications of the calibrated SIE function support its usefulness. First, single-structure based SIE calculations were tested for virtual screening (VS) enrichment against estrogen receptor (ER) and thymidine kinase (TK) showing the ability of SIE to recover true hits in a collection of decoys.[5] While the ER set is considered an easier test, the TK set is more challenging partly due to weaker binding affinities for the true binders. The SIE function was able to recover all true positives within the top 10% of the ranked data set and half of them within the top 1%. The SIE was clearly superior to simpler functions, e.g., buried surface area that describes only nonpolar effects and ranked all TK true binders near the bottom of the list.

The best way to evaluate computational methods is *via* blind tests, so SIE was a participating method in the Statistical Assessment of the Modeling of Proteins and Ligands (SAMPL), an initiative organized by OpenEye, Inc. since 2007, which provides blind assessments for protein and ligand modeling methods including solvation, tautomerism, docking, virtual screening, and affinity calculations.[16−18] We tested prospectively the calibrated SIE function in the protein−ligand binding affinity section of the SAMPL1 challenge in 2008,[19] specifically on the Jun kinase 3 (JNK3) data set, a target class not present in the SIE calibration data set. This data set consisted of 49 diverse JNK3 inhibitors from 12 classes, each with its own cocrystal structure with the kinase. The withheld binding affinities span 4.9 kcal/mol and do not correlate with the molecular weights ($R^2 = 0.02$). Also mingled in the data set were 10 models of known "inactive" ligands (in fact weakly active, with K_i or IC_{50} higher than 10 μM), which were docked in duplicated enzyme structures. Structural preparation of complexes followed the same curation as for SIE calibration, including the standard constrained minimization protocol restricted to the ligand and binding site region.[5,15] The SIE function achieved reasonable prospective predictions for the JNK3 data set of 49 known actives, with bootstrapped R^2 of 0.36, and Kendall-tau rank correlation coefficient (τ_K) of 0.42, with no other submission performing better (methods undisclosed). It was also clearly apparent that SIE can estimate absolute binding affinities, with predicted values spanning the same range as the actual ones (Figure S1B). The absolute errors for SIE predictions on the subset of actives were MUE of 0.92 kcal/mol and RMSE of 1.09 kcal/mol. These are slightly better than the null model (the mean of experimental data taken as prediction for all compounds). Encouragingly, the 10 measured "inactives" were separated reasonably well from the actives, leading to an increase in the bootstrapped R^2 and τ_K to 0.54 and 0.55, respectively, over all 59 ligands.

The SIE function has also been applied retrospectively as well as prospectively in several other independent laboratories that have reported SIE predictions versus actual binding affinities.[20−28] Collectively, these data indicate an R^2 of 0.59 between the predicted and actual absolute binding affinities (Figure S1C). As in the case of the SAMPL1 blind test, these applications reiterate that the SIE approach returns predicted protein−ligand binding affinities well within the range of experimental measurements. The degree of scatter is comparable to that observed in the original calibration, suggesting that the SIE parameters were not overfitted to the training set.

In this report, we extend the testing the SIE function to the Community-Structure−Activity Resource (CSAR) scoring challenge featuring a curated protein−ligand data set that is highly diverse with respect to the protein targets. The CSAR-2010 binding affinity scoring benchmark data set consists of high-resolution cocrystal structures for 343 protein−ligand complexes with high-quality binding affinity data. While the data set resembles the SIE calibration data set of 99 protein−ligand complexes in terms of target diversity and curation quality, there is no single entry in the CSAR-2010 data set that was present in the SIE calibration data set. Some protein targets like trypsin, HIV protease, and PTP-1B are however represented in both data sets. Also, this CSAR data set includes metal-ion−mediated protein−ligand interactions, which were absent in the SIE calibration data set, thus allowing the testing of SIE predictions for this important type of biological interactions.

Particular emphasis will be given to the sensitivity of SIE predictions to the assignment of protonation and tautomeric states and to the treatment of metal ions near the protein−ligand interface. To this end, we directed some of our efforts toward curating the CSAR-2010 data set in terms of protonation and tautomeric states in the complex and contributed the CSAR-NRC-HiQ version that is currently used by the participating community. Testing was carried out primarily for the publicly distributed original calibration of the SIE function.[5,6,15] Cross-validated retraining of physical parameters for the SIE function on the CSAR data set was also be attempted and shown here to lead to a marginal improvement in performance. This SIE benchmark is based on single-conformation representations of the complexes with prior constrained energy minimization in the active site region, which is also available in the distributed CSAR-NRC-HiQ version. In order to study the effect of conformational averaging and ligand strain, we also applied the MD-based *sietraj* mode on a sample of overestimated and underestimated SIE outliers. The generated MD trajectories were also used to compare the SIE predictions with those obtained with similar end-point approaches, including MM-PB(GB)/SA without and with entropy contributions, and LIE.

MATERIALS AND METHODS

Data Set Preparation. Structural preparation for SIE calculations resulted in two versions of the CSAR data set. A first version

is based on the first official release called CSAR-HiQ. A second version starts with the prepared CSAR-HiQ version and furthers the curation in terms of protonation, tautomerism, and proton orientation, leading to the current official release CSAR-NRC-HiQ. Both versions were refined by constrained minimization in the active site region, which is required for SIE calculations.

Preparation of the CSAR-HiQ was carried out in the same way as the preparation of the data set of 99 protein−ligand complexes used for the calibration of the SIE function.[5] This was done via an automated protocol with a combination of Tool Command Language (Tcl) and SYBYL (Tripos, Inc., St. Louis, MO) Programming Language (SPL) scripts and involved minimal visual structural examination followed by manual intervention. General curation included disulfide bond formation, retaining all metal ions, retaining unnatural and modified residues and cofactor molecules, retaining the full oligomeric state as provided (except the very large 2-257 entry that was cut down to a dimer), and chain termini reloaded for proper atom naming and charging. All water molecules were removed. Glycosylation sugar residues far from the ligands in all but one case were removed, and the corresponding Asn residues were capped with H atoms, except in entry 1-163 where one sugar residue adjacent to the ligand was retained. Minor structural corrections were made to several unnatural and modified residues upon visual inspection (Table S1), also improving consistency throughout the data set. Force field charges and atom types were assigned for both energy minimization and SIE calculations. Protein molecules were assigned AMBER parm94 atomic partial charges and atom types using SYBYL.[29−31] Ligand and cofactor molecules were assigned AM1-BCC atomic partial charges using MOLCHARGE (Openeye, Inc., Santa Fe, NM)[32,33] and GAFF atom types using ANTECHAMBER and PARMCHK in AMBER.[34−36] Unusual and modified residues were assigned AM1-BCC atomic partial charges for blocked residues and renormalized to integer net charge for residue units and assigned AMBER parm94 atom-types by similarity to the natural amino-acid residues. Metal ions were given their full net charges and AMBER-compatible parameters (Table S2).

Preparation of the upgraded CSAR-NRC-HiQ version was based on visual inspection of *all* protein−ligand complexes from the prepared CSAR-HiQ version. Changes were made at the protein−ligand interface in terms of ligand and/or protein protonation/tautomeric states, followed by recalculation of partial charges and reassignment of force-field atom types. Suitable protonation/tautomeric states of the ligand and protein residues were mainly inferred from the hydrogen-bonding pattern in the ligand-bound active site. In the case of the ligands, the feasibility of the alternate protonation was verified with PKATYPER (Openeye, Inc., Santa Fe, NM). These changes assumed no change in protonation state between the free and bound states. No acidity constants or their shifts from the expected values (pK_a, ΔpK_a), or protonation equilibria, which depend on the pH and the pK_a's of titratable groups, were calculated for any of the free and bound states. Hence, no energetic correction incurred from protonation or tautomerism was taken into account. The source and/or related literature were generally consulted when available, and in several cases the assignment of alternate protonation and tautomeric states was suggested by these reports. A listing of all protonation and tautomeric changes between the CSAR-HiQ and CSAR-NRC-HiQ versions is provided in Tables S3 and S4. Specific examples and statistics are detailed in the Results section. The CSAR-NRC-HiQ data set also included manual reorientation followed by energy minimization for specific polar H atoms that were found not optimized for H-bonding interactions upon the energy minimization started from their original orientation (as in CSAR-HiQ).

Single-conformation-based SIE calculations based on crystal structures generally require energy minimization in order to reduce the noise arising mainly from the intermolecular van der Waals interaction energy. Several minimization protocols have been previously tested, with restrained minimization of ligand heavy atoms together with unrestrained minimization of hydrogen atoms within a 4 Å per-residue sphere providing somewhat superior results than full minimization of the complex or minimization of the hydrogen atoms only.[5] A similar protocol was used in the application of SIE to the JNK-3 data set from the SAMPL1 blind challange.[19] Our current protocol, applied to CSAR-HiQ and CSAR-NRC-HiQ, includes energy minimization of the ligand and protein residues within 4 Å from the ligand, and applying harmonic restraints with force constants of 3 kcal/(mol Å^2) and 20 kcal/(mol Å^2) for the ligand and protein, respectively, heavy atoms in this region. The assigned AMBER/GAFF force-field parameters and two-stage-RESP/AM1-BCC partial charges described earlier, together with a distance dependent dielectric constant ($4r$) to crudely mimic solvent screening, were used for energy minimization down to a gradient of 0.01 kcal/(mol Å).

SIE Calculations. SIE approximates the protein−ligand binding free energy in aqueous solution, ΔG_{bind}, by an interaction energy contribution, E_{inter}, and a desolvation free energy contribution, ΔG_{desolv}.[5,6,15] Each of the interaction and desolvation contributions is further made up of an electrostatic component and a nonpolar component

$$\Delta G_{bind} \approx E_{inter} + \Delta G_{desolv} = \underbrace{E_{inter}^{Coul} + \Delta G_{desolv}^{R}}_{electrostatic} + \underbrace{E_{inter}^{vdW} + \Delta G_{desolv}^{np}}_{nonpolar} \quad (1)$$

The electrostatic SIE component includes the Coulombic intermolecular interaction energy, E_{inter}^{Coul}, and the electrostatic desolvation free energy, ΔG_{desolv}^{R}, due to the change in reaction field energy upon binding. The nonpolar SIE component includes the van der Waals intermolecular interaction energy, E_{inter}^{vdW}, and the nonpolar desolvation free energy, ΔG_{desolv}^{np}, that results from changes in the solute−solvent van der Waals interactions and changes in the work of maintaining the solute-size cavity in water. In keeping with the philosophy of the AMBER force field,[29,35,36] hydrogen-bond formation is not considered explicitly but rather treated as an electrostatic effect. Internal strain that may be incurred upon binding is typically not taken into account in the common application modes of SIE, with the free state of the system obtained from the infinite rigid separation of the protein and ligand conformations from their complexed state. Entropy is not explicitly included; however, calibration of the SIE function on binding affinities leads to an empirical overall scaling factor of the solvated potential energy, whose value corresponds to, and hence can be interpreted as, the effect of configurational entropy compensation on binding free energy.[13,14]

In order to calculate the intermolecular Coulomb and van der Waals interaction energies in the bound state, E_{inter}^{Coul} and E_{inter}^{vdW}, we use the AMBER force field,[29,36] suitable for simulation of biomacromolecules, and its extension to small molecules, GAFF.[35] Partial atomic charges for protein atoms from the AMBER force field are calculated by the two-stage RESP fitting method to the electrostatic potential at *ab initio* level,[30,31]

whereas ligands are assigned AM1-BCC partial charges,[32,33] which are a high-quality surrogate of RESP charges but faster to calculate and hence practical for virtual screening applications of SIE. The same force-field nonbonded parameters and partial charges were also used for structural refinement by energy minimization and MD simulations.

For electrostatic desolvation, the change in the reaction field energy between the bound and free states, ΔG^{R}_{desolv}, is calculated with a high-quality continuum model based on a boundary element solution to the Poisson equation using the BRI BEM program.[37,38] The molecular surface required for boundary element electrostatic calculations is generated with a marching tetrahedra tessellation algorithm,[39,40] and a variable-radius solvent probe that adjusts with respect to the polarity of each particular atom being surfaced.[41] Atomic Born radii for surface generation are based on AMBER van der Waals radii and, together with the dielectric constant, are physical parameters used to calibrate the SIE function. The same partial charges used for Coulombic calculations are also used for reaction field energy calculations. The generated molecular surface is also used to calculate the change in molecular surface area upon binding, ΔMSA. This is then used to calculate the nonpolar desolvation term, ΔG^{np}_{desolv}, based on a linear relationship between experimental hydration free energies of alkanes and their MSAs.

The following physical parameter dependence of the SIE function, at fixed molecular mechanics force-field nonbonded parameters (van der Waals and partial charges), is used

$$\mathrm{SIE}(\rho, D_{in}, \alpha, \gamma, C) = \alpha \cdot [E^{Coul}_{inter}(D_{in}) + \Delta G^{R}_{desol}(\rho, D_{in}) + E^{vdW}_{inter} + \gamma(\rho, D_{in}) \cdot \Delta MSA(\rho)] + C \quad (2)$$

Here, ρ is a factor applied to derive atomic Born radii by linear scaling of AMBER van der Waals radii (R^*). D_{in} is the solute interior dielectric constant. Both electrostatic terms, E^{Coul}_{inter} and ΔG^{R}_{desolv}, depend strongly on D_{in}, and ΔG^{R}_{desolv} also depends on Born radii (hence on ρ). γ is the molecular surface tension coefficient describing the nonpolar component of solvation free energy, ΔG^{np}_{desolv}, upon multiplication by the change in the molecular surface area of the solute upon binding, ΔMSA. The surface tension γ depends weakly on the (ρ,D_{in}) parameters, as it is derived from the experimental hydration free energy of alkanes after subtracting their small electrostatic solvation component (calculated), and fitting the pseudoexperimental nonpolar residual to their MSAs that depend on atomic radii. α is a global scaling factor of the total raw solvated interaction energy related to the scaling of the binding free energy due to configurational entropy effects.[13,14]

In this work we used the default values of $\rho = 1.1$, $D_{in} = 2.25$, $\gamma = 12.894$ cal/(mol Å), $\alpha = 0.104758$, and $C = -2.89$ kcal/mol, which were obtained by calibrating against the SIE protein−ligand training data set of 99 complexes refined by restrained energy minimization.[5] This currently distributed parameter set will be referred to as the "standard" SIE parametrization for the rest of the paper. We have also performed a cross-validated calibration of SIE on the CSAR data set, retraining the parameters on each of the two predefined halves of the data set and testing on the alternated halves. The resulting parameters sets will be referred to as the "refitted" SIE parametrization in the paper.

MD Simulations. Thirteen complexes from CSAR-NRC-HiQ having underestimated or overestimated affinities by single-conformation based SIE calculations were selected for MD simulations in explicit water using AMBER 10,[36,42] in order to enable *sietraj*, ligand strain, MM-PB(GB)/SA, and LIE calculations. Each structure was solvated in a truncated octahedron TIP3P water box extending 12 Å around solute,[43] and electroneutrality was achieved by adding Na^+ or Cl^- counterions. Classical MD simulations were carried out under the AMBER force field with the FF99SB parameters for the proteins,[44,45] and GAFF parameters and AM1-BCC partial charges for the ligands.[32,33,35] Appropriate force field atom types for the ligands were assigned with ANTECHAMBER.[34] Thus, the force field atom-typing and atomic partial charges are identical to those used in the single-conformation based SIE calculations for these complexes. Applying harmonic restraints with force constants of 20 kcal/(mol Å^2) to all solute atoms, each system was energy-minimized first, followed by heating from 100 to 300 K over 25 ps in the canonical ensemble (constant number of particles, volume, and temperature, NVT) and subsequently equilibrating to adjust the solvent density under 1 atm pressure over 25 ps in the isothermal−isobaric ensemble (constant number of particles, pressure, and temperature, NPT) simulation. The harmonic restraints were then gradually reduced to 0 with four rounds of 25-ps simulations. A 3-ns production NPT run was obtained for each complex, with snapshots collected every 1 ps, using a 2-fs time step and 9-Å nonbonded cutoff. Production runs were extended up to 6 ns for the overestimated complexes. Production runs of 2 ns were also obtained for the free uncomplexed ligands from separate MD simulations. The Particle Mesh Ewald method was used to treat long-range electrostatic interactions,[46] and bond lengths involving bonds to hydrogen atoms were constrained by SHAKE.[47] Standard analyses of MD trajectories were carried out with PTRAJ in AMBER 10, which indicated that the MD simulations attained structural convergence.

Sietraj and Ligand Strain Calculations. Average SIE values were calculated with the *sietraj* program, which carries out SIE calculations for selected conformations of the complex extracted from an MD trajectory.[6,15] Averages were taken over 50 uniformly spaced snapshots from the last ns of each simulation.

Using separate trajectories for the complex and the free ligand, we also calculated the average solvated conformational energy (SCE), which includes the internal strain energy of the ligand, E^{AMBER}_{ligand}, as well as the change in electrostatic and nonpolar solvation of the ligand between its free-state ensemble and the bound-state ensemble

$$\mathrm{SCE}_{ligand}(\rho, D_{in}, \alpha, \gamma) = \Delta\langle\alpha \cdot [E^{AMBER}_{ligand}(D_{in}) + G^{R}_{ligand}(\rho, D_{in}) + \gamma(\rho, D_{in}) \cdot MSA_{ligand}(\rho)]\rangle \quad (3)$$

where α, γ, ρ, and D_{in} physical parameters correspond to those in eq 2 and take the values from the original SIE parametrization. The difference Δ is calculated between the average SCE values calculated on the ligand trajectory extracted from complex trajectory, and on the free ligand trajectory. The average ligand strain contribution, SCE_{ligand}, can be optionally added to the average SIE contribution from the MD simulation (i.e., to the *sietraj*). The same snapshots as for the *sietraj* calculations were used.

MM-PB(GB)/SA and Entropy Calculations. Estimates of binding affinity using the MM-PB(GB)/SA methods,[6−9] were

calculated in AMBER 10 from a single trajectory, that of the complex, which cancels all internal energy term and reduces to the following expression

$$\Delta G_{bind} \approx \langle (\Delta E^{vdW} + \Delta E^{Coul} + \Delta G^{elec}_{solv} + \Delta G^{np}_{solv} - T\Delta S) \rangle \quad (4)$$

where the differences Δ are taken between the bound state and the free state for a given snapshot in the trajectory, and then the average is taken over a number of snaphots. The same snapshots as for the *sietraj* calculations were used. In the single-trajectory approach, the free state is obtained from rigid separation of the complex trajectory into a protein trajectory and a ligand trajectory, with the explicit solvent and counterions being replaced by a continuum dielectric model. This mirrors directly the approach taken for *sietraj* calculations. In addition to the molecular mechanics force-field terms for van der Waals and Coulomb electrostatic interactions, E^{vdW} and E^{Coul}, respectively, the electrostatic component of solvation, G^{elec}_{solv}, is obtained by solving the GB equation[48] or by calculating reaction field energies using the finite-difference method to solve the Poisson−Boltzmann equation.[49] Dielectric constants for solute and solvent are set to 1 and 80, respectively. The nonpolar solvation contribution, G^{np}_{solv}, is estimated as $\gamma \cdot$ SASA,[50] with the solvent-accessible surface area (SASA) determined using a water probe radius of 1.4 Å, and given a surface tension coefficient γ of 0.0072 kcal/(mol Å^2).

In eq 4, T and S are the temperature and the total solute entropy, which consists of translation, rotation, and vibration entropies, which were also calculated in AMBER 10. Translation and rotation solute entropies are calculated analytically for each snapshot using the Sackur-Tetrode equation,[51] and the vibrational entropy contributions are estimated by classical statistical thermodynamics using normal-mode analysis.[51] To obtain the normal modes, we carried out minimization of each snapshot in gas phase using the conjugate gradient method with a distance-dependent dielectric constant of 4r, until the rms of the elements of the gradient vector was less than 10^{-4} kcal/(mol Å). Due to the high computational demand in the minimization steps required for normal-mode analysis, average vibration entropies were based on 6 snapshots over the last ns of each simulation.

LIE Calculations. Based on the separate MD trajectories for the complex and the free ligand, we applied the linear interaction energy (LIE) approximation to binding free energy,[11,52,53] which is based on ligand interactions with its environment in the bound and free states

$$\Delta G_{bind} \approx \alpha \cdot \Delta\langle E^{vdW} \rangle + \beta \cdot \Delta\langle E^{Coul} \rangle + \Delta\langle G^{RF}_S \rangle_{12Å\text{-}\infty} \quad (5)$$

where the differences Δ are calculated between the average values in the solvated complex minus the average value in the solvated free ligand. The scaling coefficients α = 0.18 and β = 0.43 for the change in the average van der Waals and Coulomb electrostatic interactions energies of the ligand with its environment, $\Delta\langle E^{vdW} \rangle$ and $\Delta\langle E^{Coul} \rangle$, respectively, are taken from the previous calibration of the LIE method.[11,54] Solvation effects are described with the explicit model used in the MD simulation (TIP3P water), hence these terms include ligand interaction energies with explicit water molecules, which are calculated up to 12 Å around the ligand. An average continuum correction to electrostatic solvation beyond the sphere of explicit water to infinity, $\langle G^{RF}_S \rangle_{12\ Å\text{-}\infty}$, is also applied as described elsewhere.[55]

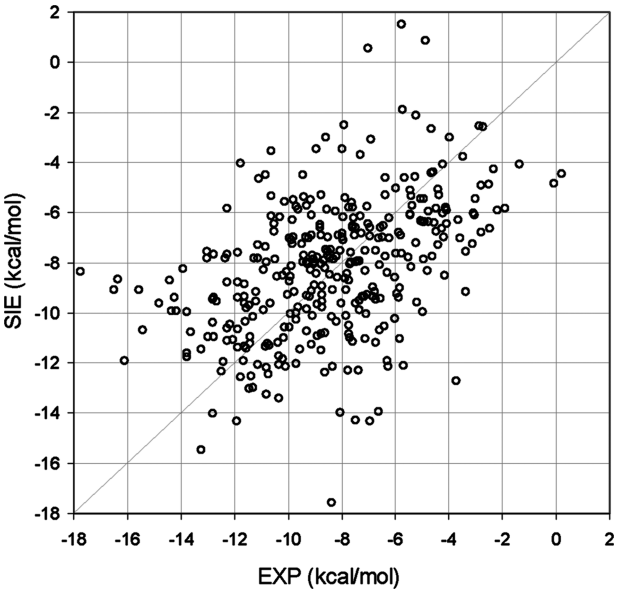

Figure 1. Scatter plot between experimental binding affinities and SIE values calculated with the standard parametrization on the CSAR-HiQ preparation.

The same snapshots as for the *sietraj* and MM-PB(GB)-SA calculations were used for LIE calculations.

RESULTS

SIE Predictions on the Automatically Prepared CSAR-HiQ Version. Predictions using the standard SIE parametrization[5,6,15] are plotted versus the experimental values in Figure 1, with the statistical performance assessed in Table 1. First, it is apparent that the SIE-predicted binding affinities span the same range as the actual ones. However, there is significant scatter in Figure 1, which is mirrored by MUE and RMSE values which are similar to the null model (Table 1). In addition, we noted that the nonpolar terms alone, the intermolecular van der Waals interaction energy, E^{vdW}_{inter}, or the buried molecular surface are upon complexation, ΔMSA, while not being able to account quantitatively for absolute binding affinities, do provide better correlations with the actual binding affinities than the full SIE function. These results obtained on the CSAR-HiQ version indicate that the electrostatic terms, including direct interactions and desolvation, introduce significant noise into the SIE function, being primarily responsible for the standard SIE performance not improved from the null.

Upon half−half cross-validated refitting of physical parameters of the SIE function on CSAR-HiQ, the performance improved considerably, with MUE and RMSE values lower than the null model (Table 1). However, in correlative terms the performance of the whole refit SIE function was practically identical to that of the E^{vdW}_{inter} term alone, suggesting that the refit effectively excluded the electrostatic terms and retained only the nonpolar signal. Examination of the new sets of optimal parameters derived on CSAR-HiQ (Table S5) showed that the most significant change in optimal parameters relative to the standard SIE parametrization was the increase in optimal D_{in} from 2.25 to 7, in fact the highest value scanned in this study. At this or higher D_{in}, both electrostatic terms E^{Coul}_{inter} and ΔG^{R}_{desolv} have very small

Table 1. Statistical Performance of the SIE Function on the CSAR Data Set

			CSAR-HiQ		CSAR-NRC-HiQ	
statistical index	null model[i]	Δ*MSA* model[j]	standard SIE model	refit and test SIE model	standard SIE model	refit and test SIE model
MUE[a]	2.423		2.408	1.894	1.985	1.835
RMSE[b]	3.037		3.104	2.408	2.487	2.310
RmSE[c]	2.027		2.004	1.612	1.767	1.590
ρ_S[d]		0.606	0.473	0.631	0.617	0.659
τ_K[e]		0.428	0.324	0.444	0.437	0.471
R^2[f]		0.357	0.188	0.382	0.375	0.425
$R^2_{(b=0)}$[g]			−0.033	0.380	0.354	0.425
$a_{(b=0)}$[h]			0.963	1.035	0.948	1.021

[a] Mean-unsigned-error, in kcal/mol. [b] Root-mean-square-error, in kcal/mol. [c] Root-median-square-error (same as median-unsigned-error), in kcal/mol. [d] Spearman-rho rank correlation coefficient. [e] Kendall-tau rank correlation coefficient. [f] Pearson squared correlation coefficient. [g] Pearson squared correlation coefficient with the intercept, *b*, set to zero, for the correlation $\Delta G_{exp} = a \cdot \mathrm{SIE} + b$. [h] Slope, *a*, for the correlation $\Delta G_{exp} = a \cdot \mathrm{SIE} + b$, when $b = 0$. [i] Mean experimental value in the CSAR data set as prediction of binding affinities. [j] Similar values are obtained on the CSAR-HiQ and CSAR-NRC-HiQ versions.

nominal contributions to the SIE function, confirming the exclusion of electrostatic terms in the refitted SIE on CSAR-HiQ.

These results prompted us to have a closer look at the two types of major outliers that can be identified by standard SIE on the CSAR-HiQ data set. For many underestimated outliers, close visual examination of the protein−ligand interface revealed deficiencies in the assignment of protonation and/or tautomeric states of the ligand and/or protein. The other class representing largely overestimated outliers included negatively charged ligands (typically with phosphate groups) in contact with metal ions. These distinct characteristics of both underestimated and overestimated outliers relate directly to the electrostatic component of binding. Hence, the outlier analysis revealed deficiencies in the CSAR-HiQ data set and provided the hypothesis that further curation of the data set would improve the electrostatic signal with the SIE function.

Sensitivity of SIE Predictions to Protonation. In order to curate protonation and tautomeric states, we assessed the protein−ligand interfaces of *all* 343 complexes in the CSAR-HiQ data set, not only of the SIE outliers. As described in the Materials and Methods section, assignment of protonation and tautomeric states of the ligands and protein binding sites was done mainly by assessing the feasibility for hydrogen-bonding interactions and the ability of the ligand to exhibit alternate states, together with consulting the relevant published literature.

Although one characteristic of the CSAR data set is the diversity of proteins, there are several series of relatively congeneric ligands binding to the same protein or to a group of closely related proteins. For three such series, we could identify "generic" protonation changes based on literature data. These series includes 9 sulfonamide inhibitors of carbonic anhydrase (CA) homologues, 28 inhibitors of HIV protease (HIVP) and its aspartic protease (AP) homologues, and 9 inhibitors of protein tyrosine phosphatase (PTP). It is well accepted that the sulfonamide moiety of CA inhibitors interacts with the Zn^{2+} ion in the CA active site in deprotonated form.[56,57] Hence, the sulfonamide group was deprotonated in all these ligands bound to CA homologues. It is also known that in the HIVP dimer, one of the two active site Asp residues is protonated, except when the inhibitors bind to the active site directly with a positively charged moiety.[58−60] Hence, in 26 of the 28 complexes of HIVP and AP, one of the two Asp25 residues was protonated. It is known that the active site Cys residue of a PTP possesses a nucleophilic thiolate group stabilized by positive charges from adjacent residues.[61,62] Hence, the Cys215 residue of PTP-1B was deprotonated in all its complexes with inhibitors. These generic protonation changes to the CSAR-HiQ version generally improved SIE predictions of absolute binding affinities, with a typical example from each series shown in Figure 2.

Required changes in the protonation and/or tautomeric state were identified for a large number of ligands in the CSAR-HiQ preparation version, which are documented in Table S3, with a sample detailed in Figures 3A and S2A. In entry 1-99 for example, based on distance measurements in the complex, it is clear that a positively charged amidinium-like moiety bearing protons on both N atoms is required on the ligand molecule, which is also a feasible protonation state at neutral pH. Using the protonated amidinium form dramatically improved the underestimated SIE prediction relative to the neutral form, in which two partially negatively charged atoms, an N atom of the ligand and a carbonyl O atom, of the protein are facing each other at an H-bonding distance of 2.84 Å (all distances are based on crystal structures). Similarly for entry 2-222, the unsubstituted N atom of the imidazolyl moiety of the ligand faces a carboxylate O atom of the protein at 2.74 Å. The protonated imidazolium cation, suitable for H-bonding to the Asp side-chain and a populated state at neutral pH, improved SIE prediction relative to the neutral state. In entry 2-89, there are three N atoms of the aminoquinazolinone ligand engaged in four H-bonding contacts with two Asp residues of the protein. Protonation of the ligand to the charged amidinium form improves the SIE prediction relative to the neutral state with electrostatic repulsion at one of the four N−O contacts. While some of the protonation states in the CSAR-HiQ version are atom-typing errors (e.g., the glycine ligand in the entry 1-173), others have deeper sources of errors, sometimes rooted in the ligand annotation in PDB (e.g., double bond reduction is required prior to the protonation of the secondary amine of the propranolol ligand in entry 2-44). The vast majority of the protonation/tautomerism changes improved SIE prediction. We also found cases where the protonation state required by the H-bonding network worsened SIE predictions. For consistency, these changes were made regardless of their outcome on SIE predictions. An example is entry 2-176, where the citric acid ligand faces with one of its carboxylate groups the

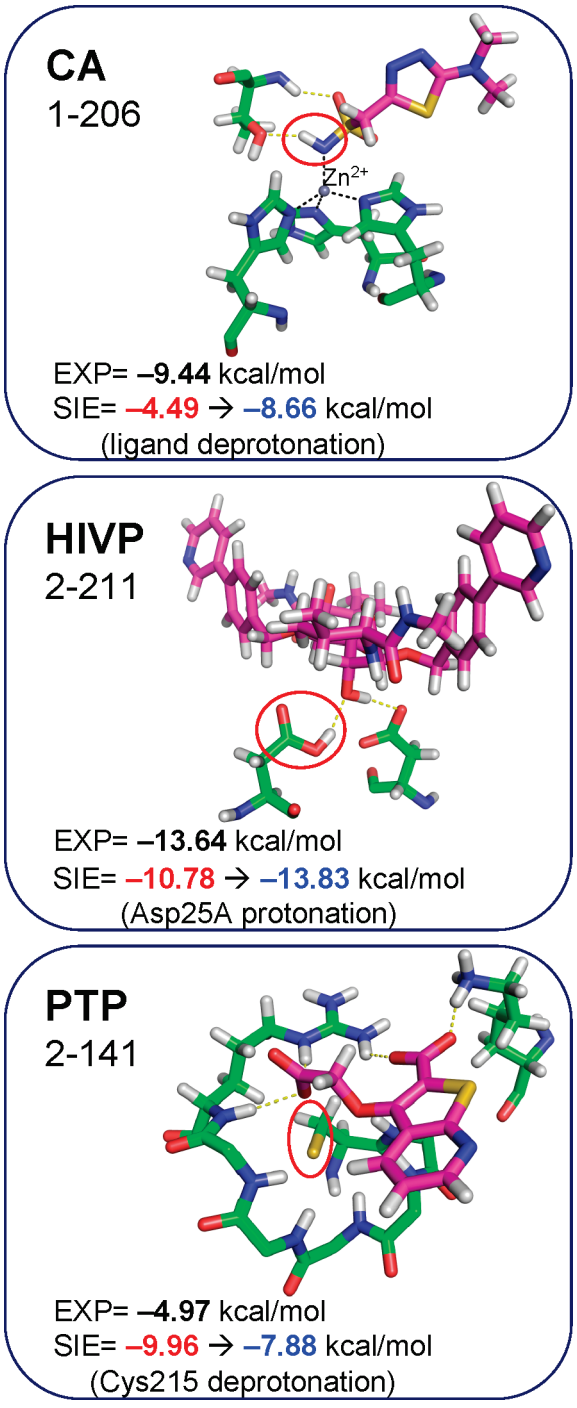

Figure 2. Typical examples from generic changes in ligand or protein protonation state. CA: carbonic anhydrase, HIVP: HIV protease, PTP, protein-tyrosine-phosphatase 1B. The CSAR ID numbers are given. The C atoms of ligands are shown in magenta, and C atoms of displayed protein residues are shown in green. H-bonds are shown with yellow dotted lines. The sites of protonation change are indicated with red ovals. The standard SIE values before the change (CSAR-HiQ) are in red; those after the change (CSAR-NRC-HiQ) are in blue.

carboxylic group of an Asp residue in the binding site, at a short H-bond distance (2.48 Å in the crystal structure). Our analysis suggested protonation of that carboxylate group of the ligand, which worsened an otherwise reasonable SIE prediction. It is possible that the worsened prediction in this case is related to ignoring changes in protonation state that may occur between the free and bound states. Overall, 46 complexes (13% of the CSAR data set) were affected by changes in protonation/tautomeric state of their ligands. Previously underestimated complexes were largely corrected (Figure 3C), with a mean-signed-error (MSE) for these complexes lowered from 2.13 (indicating underestimation) to −0.09 kcal/mol. In terms of absolute errors of standard SIE, there is a marked reduction of the overall MUE from 3.14 to 1.79 kcal/mol after correction, most improvements affecting the major outliers, and minor deterioration in predictions occurring for reasonably predicted complexes (Figure 3B).

A similar analysis identified an even larger number of protonation/tautomerism changes required on the protein side in the CSAR-HiQ preparation (Table S4). A few illustrative examples (entries 2-101, 1-168, 1-34) are given in Figures 4A and S2B. Interactions with the phosphate group of the ligand in entry 2-101 require for a His side-chain not only a tautomeric change for establishing an H-bond at the distance of 2.97 Å but also a charged form due to the likely increase in its pK_a by the proximal phosphate group. This change applied to entry 2-101 improved SIE prediction of absolute binding affinity. Likewise, in entry 1-168 an Asp carboxylate group of the protein faces a phosphate group from the ligand at an H-bonding distance of 2.80 Å, requiring a proton on one of these interacting groups. We chose to protonate the protein carboxylate, which improved the SIE prediction. Modification of tautomeric states of two His residues for improved H-bonding network in entry 1-34 had no effect on the SIE prediction, possibly due to the fact that the intramolecular H-bonding (His-Gln), and not the protein−ligand interactions, benefited most from these changes. For the exemplified entries 2-101, 1-34, and 1-168, there were further small improvements in SIE predictions upon reorientation of a few polar H atoms at the protein−ligand interfaces, a topic discussed in the next paragraph. In general, improvements in SIE predictions were larger upon changing protonation states than tautomeric states, which relates directly to changes in the signal carried by the electrostatic terms, as well as to the lack of an explicit H-bond treatment in the SIE function. Overall, 68 complexes (20% of the CSAR data set) were affected by changes in the protonation/tautomeric state of their proteins. The mild underestimation of some of these complexes is corrected (Figure 4C), reflected by an overall reduction in MSE from 1.30 (indicating underestimation) to 0.35 kcal/mol. There was a reduction of the overall MUE for these complexes from 2.52 to 1.94 kcal/mol after correction, with standard SIE predictions corrected partially for the major outliers and fully for several mild outliers. A few entries were not affected by corrections, while other suffered minor deteriorations in standard SIE predictions (Figure 4B). The overall improvement afforded by protonation/tautomerism changes on the protein side was smaller than that from the ligand side, even though more proteins than ligands were affected by changes.

We noted that after energy minimization, a few polar H atoms did not establish optimal H-bonding interactions. Manual correction of these cases and reminimization allowed us to assess the sensitivity of the SIE function to the position of one or a few polar H atoms in these complexes. A few typical examples (entries 2-226, 1-208, 2-81) are given in Figures 5A and S2C, with a listing of all affected complexes given in Table S6. Overall, for 77 complexes where such changes were carried out, there was no change in the performance in standard SIE predictions, with

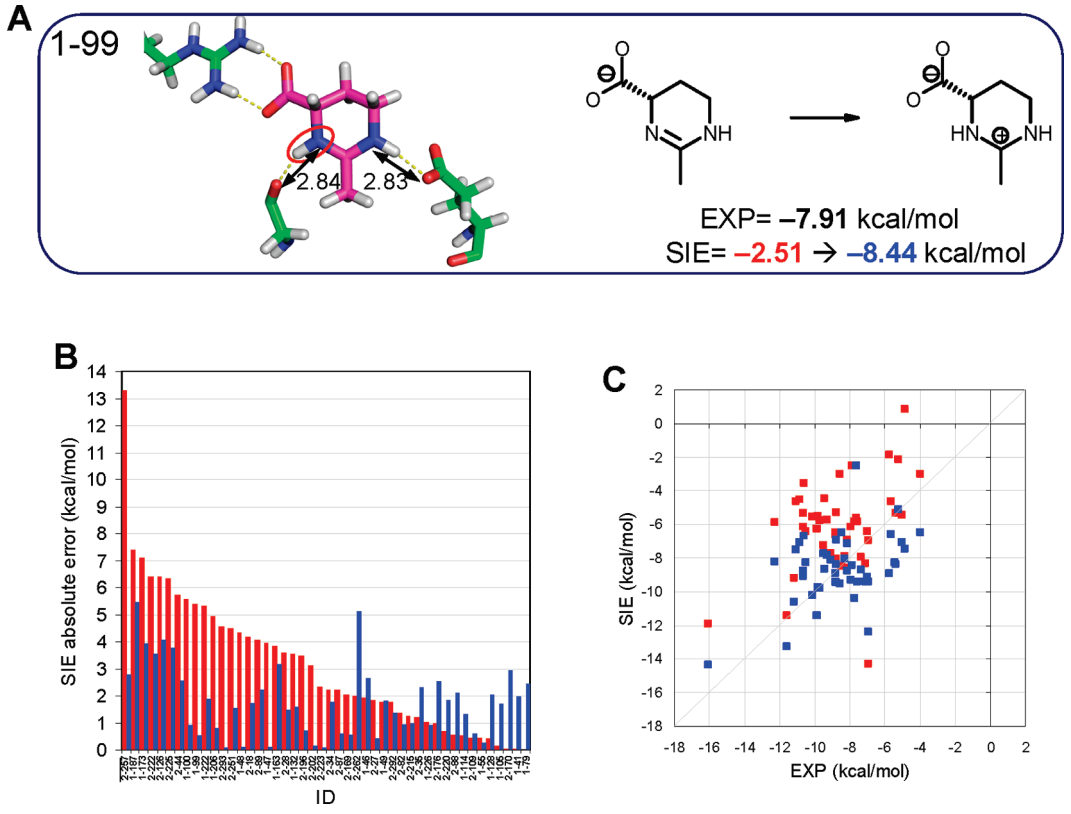

Figure 3. Sensitivity of the SIE function to ligand protonation. (A) Typical example of ligand protonation change (additional examples given in Figure S2A). Rendering color-code is as in Figure 2. Protein−ligand donor−acceptor H-bonding distances are labeled in Å units. (B) Absolute SIE errors before (red bars, CSAR-HiQ preparation) and after (blue bars, CSAR-NRC-HiQ preparation) changes in ligand protonation for the 46 affected complexes (also listed in Table S3). (C) Scatter plot of experimental binding affinities versus SIE values calculated before (red symbols) and after (blue symbols) changes in ligand protonation for the 46 affected complexes.

MUE values of 2.35 and 2.32 kcal/mol for these complexes before and after the change, respectively. This is due in part to cancellation of SIE changes in this subset upon proton orientation changes. The SIE predictions become generally more negative (stronger binding) upon improving the H-bond network (Figure 5C), due to the strengthening of the overall electrostatic contribution in the SIE function. Noteworthy, in some cases such small structural changes can lead to significant effects in the order of 1-2 kcal/mol (Figure 5B).

Sensitivity of SIE Predictions to Bridging Metal Ions. Most of the outliers severely overestimated by standard SIE on the CSAR-HiQ preparation were negatively charged ligands in contact with metal ions. While there were complexes with bridging metal ions predicted well by standard SIE, we noted that the defining characteristic of these overestimated complexes was that their metal ion is only loosely bound to the protein, while it interacts well with the ligand. By "loosely bound" we mean that the metal ion is still somewhere in the vicinity of the protein−ligand interface but no more than two chelating atoms of the protein are within 4 Å from it. In these cases, it is unlikely that the metal ion will remain bound to the protein in the absence of the ligand, while the free ligand may already have the metal ion prebound. Therefore, for SIE calculations on these systems, it is more appropriate to assign the metal ion to the ligand molecule rather than to the protein molecule as we had automatically assigned in the CSAR-HiQ version. Through visual analysis of all CSAR complexes we identified 10 such cases, most of which involve ligand phosphate groups and bivalent metal ions (Table S7). Illustrative cases (entries 1-170, 1-134, 1-225) are shown in Figures 6A and S2D. For example, phosphate O atoms from the GTP derivative in entry 1-170 chelate a Mn^{2+} ion at 2.1 Å and 2.3 Å, but the Mn^{2+} ion, although in the vicinity of the protein, is farther than 4 Å away from any chelating group of the binding site. Reassigning the metal ion with the ligand instead of the protein significantly corrected a severely overestimated SIE prediction to a value close to the actual binding affinity. A similar metal ion bridging topology is seen for entry 1-134 involving a Mg^{2+} ion tightly bound to the phosphate group of the UMP ligand but loosely bound to the protein; a significant improvement is obtained in the SIE prediction by assigning the metal ion with the ligand. In entry 1-225, although the Mg^{2+} ion is chelated by one protein atom at 2.1 Å, this may still not be sufficient to keep the metal ion bound to the protein in the absence of the ligand. The large improvement in SIE prediction obtained by assigning the metal ion to the ligand versus protein confirms this assumption.

Out of these selected complexes, only one showed practically no change in the prediction, being predicted well irrespective of the ion assignment to the protein or ligand (<1 kcal/mol error). This entry, 1-201, is the only complex in this subset that involves a monovalent ion, K^+ (Table S7) and the weaker ligand-ion electrostatic interactions may explain why the affinity was not overestimated as much when the ion was assigned with the protein. Overall, for the 10 complexes (3% of the CSAR data set)

dx.doi.org/10.1021/ci2000242 |J. Chem. Inf. Model. 2011, 51, 2066–2081

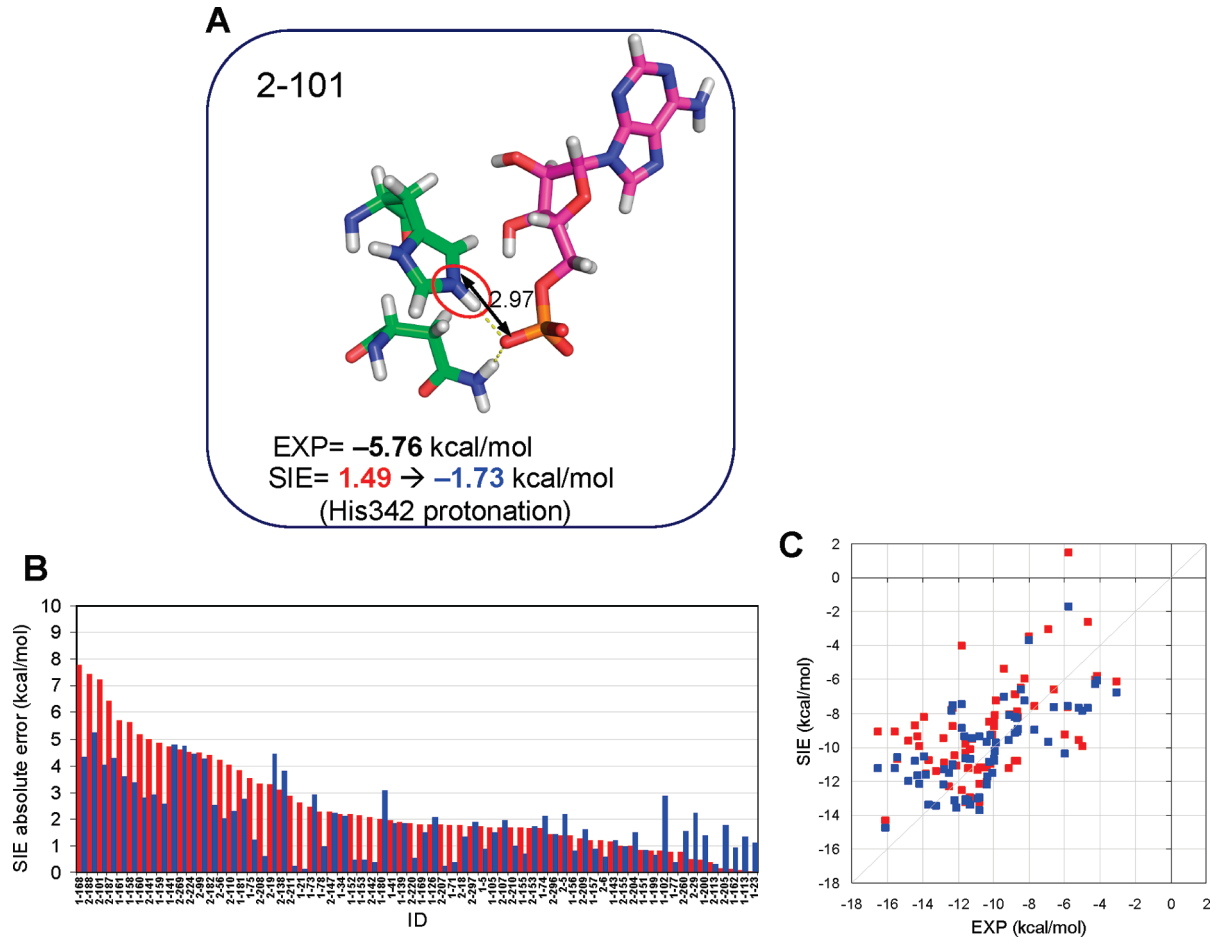

Figure 4. Sensitivity of the SIE function to protein protonation. Rendering and labeling as in Figure 3. (A) Typical example of protein protonation change (additional examples given in Figure S2B). (B) Absolute SIE errors before and after changes in protein protonation for the 68 affected complexes (also listed in Table S4). (C) Scatter plot of experimental binding affinities versus SIE values calculated before and after changes in protein protonation for the 68 affected complexes.

with reassignment of metal ions to ligands, we obtained a large improvement of standard SIE predictions of absolute binding affinities, including correction of previously overestimated complexes (Figure 6C) from an MSE of −5.30 (indicating overestimation) to −0.66 kcal/mol. Absolute SIE errors for these complexes were markedly reduced from an overall MUE of 5.30 to 1.23 kcal/mol after correction, with most improvements occurring for the major outliers (Figure 6B). Since the metal ion appears loosely bound to the protein in these systems, we also calculated the SIE values after completely removing the metal ions. This led to an MUE of 3.42 kcal/mol, hence better than the SIE predictions with the metal ion assigned to the protein but worse than with the metal ion assigned to the ligand, suggesting that the metal ion may indeed be prebound to the free ligand prior to ligand binding to the protein.

SIE Predictions on the Upgraded CSAR-NRC-HiQ Version. A summary of the improvements afforded by changes brought to the CSAR-HiQ version to generate the CSAR-NRC-HiQ version of the data set are listed in Table 2. It can be seen that the largest overall improvements in predictions with standard SIE function were obtained after changes in the ligand protonation/tautomerism and in the metal ion assignment to the ligand for complexes with bridging metal ions loosely bound to the protein. Changes in the protonation/tautomeric state of the protein binding site had a more modest impact on the overall performance, while orientation of polar H atoms beyond that provided by energy minimization had practically no impact on the overall performance. Most of the improvements in SIE predictions occurred for the major outliers from the CSAR-HiQ preparation (Figure S3).

The predictions of absolute binding affinities with the standard SIE function on the upgraded CSAR-NRC-HiQ version of the data set are plotted in Figure 7, with values listed in Table S8. With the exception of three noted outliers involving two avidin−biotin complexes (entries 1-116, 1-130) and one metal-ion mediated complex (entry 2-139), the major outliers from the standard SIE predictions on the CSAR-HiQ version (Figure 1) are largely corrected. This underscores the requirement for careful preparation of the data set with respect to the underlying chemistry in order to enable meaningful evaluation of the SIE function. It also highlights the sensitivity of the SIE function to these structural and chemical details. Quantitatively, the standard SIE function achieves a performance of slightly below 2 kcal/mol MUE (~2.5 kcal/mol RMSE) with a correlation R^2 of 0.38 (ρ_S of 0.62). This performance on the CSAR-NRC-HiQ version is clearly superior to that on the CSAR-HiQ version and also superior to the null model (Table 1). In correlative terms, the complete SIE function performs only

dx.doi.org/10.1021/ci2000242 |J. Chem. Inf. Model. 2011, 51, 2066–2081

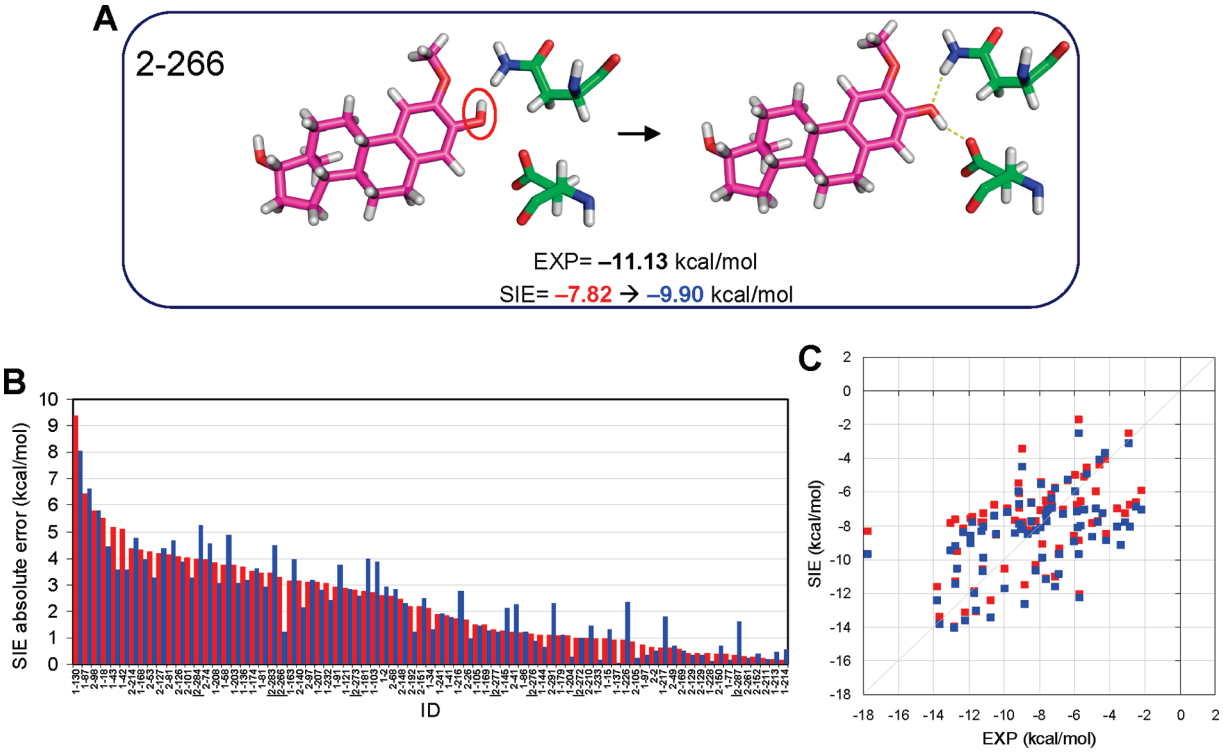

Figure 5. Sensitivity of the SIE function to orientation of a few polar H atoms. Rendering and labeling as in Figure 3. (A) Typical example of changes in the orientation of polar H atoms at the protein—ligand interface (additional examples given in Figure S2C). (B) Absolute SIE errors before and after changes in orientation of polar H atoms for the 77 affected complexes (also listed in Table S6). (C) Scatter plot of experimental binding affinities versus SIE values calculated before and after changes in orientation of polar H atoms for the 77 affected complexes.

slightly better than the nonpolar terms alone but has the advantage of accounting for absolute binding affinities (Figure 7), also highlighted by the correlation coefficient and slope when the intercept is forced through origin (Table 1). We also note that the correlation between these SIE values and the molecular weight of the ligands has an R^2 of 0.42, while the correlation of experimental binding affinity values with ligand molecular weight gives an R^2 of 0.25 (Figure S4). This indicates that the SIE function has a size bias slightly larger than that of the actual binding affinity. This size bias arises from the nonpolar terms of SIE (eqs 1 and 2), which correlate highly with the ligand size (R^2 of 0.82). We stress again that these results are obtained with the standard set of SIE physical parameters originally calibrated on a diverse data set of 99 complexes that are different than those in the CSAR data set,[5] and therefore these results represent a true test for the performance of the standard SIE function.

We also refitted the physical parameters of the SIE function on each of the two predefined halves of the CSAR-NRC-HiQ version of the data set and tested the optimal parameters on the alternate halves. As seen in Table 1, there is only a small improvement of performance with the refitted SIE function versus the standard function. This is encouraging in terms of the generality of the standard SIE parameters that are publicly available. It also indicates that the calibration of the standard SIE function was not overfitted to the original training data set. Therefore, the general use of the SIE physical parameters refitted on CSAR-NRC-HiQ is not warranted. Their optimal values do not differ much from those of the standard SIE calibration (Table S5), although the optimal D_{in} around 4 obtained using the CSAR-NRC-HiQ data set is noteworthy, being not only meaningful in terms of the dielectric constant of the protein but also in sharp contrast with a D_{in} of at least 7 obtained from the SIE refit on the CSAR-HiQ preparation. This underlines the retention of electrostatic component in the SIE function and the requirement for advanced structural curation for the development and evaluation of force field—based scoring functions.

Further Analysis of a Sample of Outliers. An effort was made to investigate the SIE outliers from the CSAR-NRC-HiQ data set. The following were considered as possible sources of prediction errors: (1) lack of explicit sampling in the single-conformation SIE application mode tested, (2) lack of internal strain energies from the SIE function, (3) the specific SIE implementation relative to other end-point methods, (4) crude estimation of entropic effects, and (5) continuum rather than an explicit treatment of the solvent.

To address the first point, we selected about a dozen of SIE outliers (both overestimated and underestimated) and run MD simulations in explicit water using the AMBER force field and then applied *sietraj* on the MD-generated conformational ensembles.[6] For reasons of simulations efficiency and results interpretability, the selected complexes do not exceed a certain size and do not include metal ions, cofactors, and unnatural or modified residues. For these entries, we found that the SIE predictions averaged over conformations extracted from MD trajectories did not improve relative to SIE predictions based on single-conformation energy-minimized complexes (Figure 8A, Table 3). These results were based on data collected over the third ns of each MD production run. We also collected data from the sixth ns of production runs for overestimated complexes and found no improvement with increased simulation time (data not shown).

dx.doi.org/10.1021/ci2000242 |*J. Chem. Inf. Model.* 2011, 51, 2066–2081

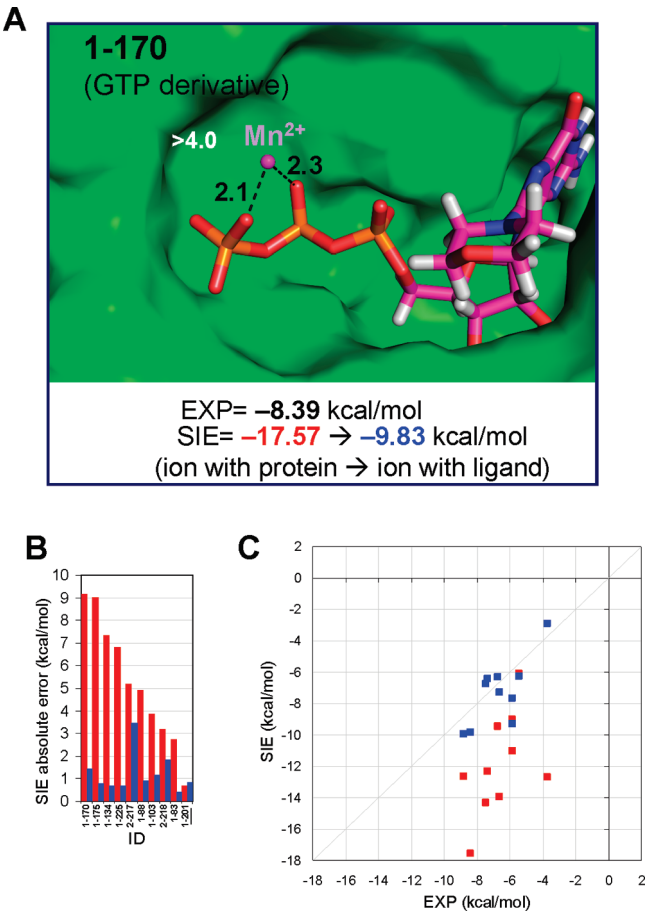

Figure 6. Sensitivity of the SIE function to the specific assignment of metal ions to the protein or ligand. (A) Typical example of a case of assignment of the metal ion to the ligand (additional examples given in Figure S2B). The protein is rendered as a solid green molecular surface, the ligand with sticks, and the metal ion as a magenta sphere. Metal-chelating interactions are shown with dashed black lines and labeled in Å units. A distance of at least 4 Å is also indicated to any other solute atom. (B) Absolute SIE errors before and after assignment of metal ions from being part of the protein (red bar, CSAR-HiQ preparation) to being part of the ligand (blue bars, CSAR-NRC-HiQ preparation) for the 10 affected complexes (also listed in Table S7). (C) Scatter plot of experimental binding affinities versus SIE values calculated before and after assignment of metal ions from being part of the protein (red symbols) to being part of the ligand (blue symbols) for the 10 affected complexes.

To address the second point, we additionally run MD simulations for the free ligands in the same conditions. This allowed us to calculate the solvated conformation energy of the ligand, SCE_{ligand} (eq 3), consisting of the average internal strain energy of the ligand between the ensembles adopted in the free and bound trajectories and including the associated change in ligand solvation. The calculated SCE_{ligand} values can adopt both signs (i.e., most often costs, but also gains due to the solvation component) and are much smaller than the corresponding SIE values. We found that predictions did not improve by simply adding the SCE_{ligand} to average SIE values (Figure 8A, Table 3). A future experiment will be to calibrate the physical parameters ($\alpha, \gamma, \rho, D_{in}$ in eqs 2 and 3) in a self-consistent manner for both of SCE_{ligand} and SIE functions, which was not attempted in this study.

Table 2. Summary of Improvements in SIE Predictions by Type of Change between CSAR Data Set Preparations

		CSAR-HiQ		CSAR-NRC-HiQ		
change	N (%)[a]	MSE[b]	MUE[c]	MSE[b]	MUE[c]	ΔCUE[d]
ligand protonation	46 (13)	2.13	3.14	−0.09	1.79	62.0
protein protonation	68 (20)	1.30	2.52	0.35	1.94	39.2
H orientation	77 (22)	0.26	2.35	−0.32	2.32	2.5
metal ion assignment	10 (3)	−5.30	5.30	−0.66	1.23	40.7
total[e]	182 (53)	0.79	2.80	−0.12	2.01	144.4

[a] Number of complexes, expressed in parentheses as percentage of the entire data set. [b] Mean-signed-error, in kcal/mol. [c] Mean-unsigned-error, in kcal/mol. [d] Change in cumulative unsigned error (CUE) of predictions between the CSAR-HiQ and CSAR-NRC-HiQ versions. [e] Overlaps removed.

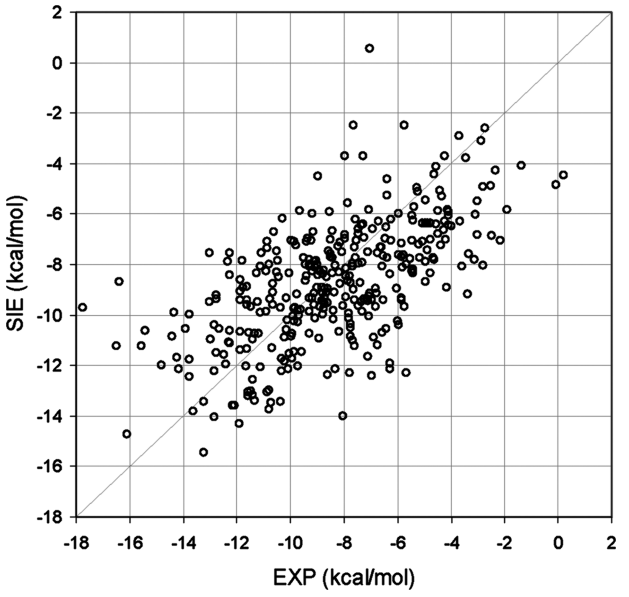

Figure 7. Scatter plot between experimental binding affinities and SIE values calculated with the standard parametrization on the CSAR-NRC-HiQ preparation.

For the third point, we subjected the MD-trajectories of the complexes to single-trajectory MM-PB(GB)/SA calculations (eq 4),[7−9] which are similar in spirit with *sietraj*.[42] We obtained a further deterioration of the outliers, with predicted affinities significantly off the range of the experimental values, and also with weaker correlations than with the single-conformation or *sietraj* implementations of the SIE method (Figure 8B, Table 3). This was not a totally surprising result, since this has been noted before.[6,21,27] For these outliers, the magnitudes of predicted affinities were improved after adding the calculated rotation, translation, and vibration binding entropy contributions, $T\Delta S_{rtv}$, to the MM-PB(GB)/SA energies. A few outliers improved slightly relative to the *sietraj* predictions, but predictions remained significantly worse for the other outliers (Figure 8C, Table 3). In correlative terms, the implementation with the more approximate GB method provided somewhat better results than the more rigorous PB method.

Finally, having calculated separate MD trajectories for the complex and the free ligand, we applied the LIE method.[11,52,53]

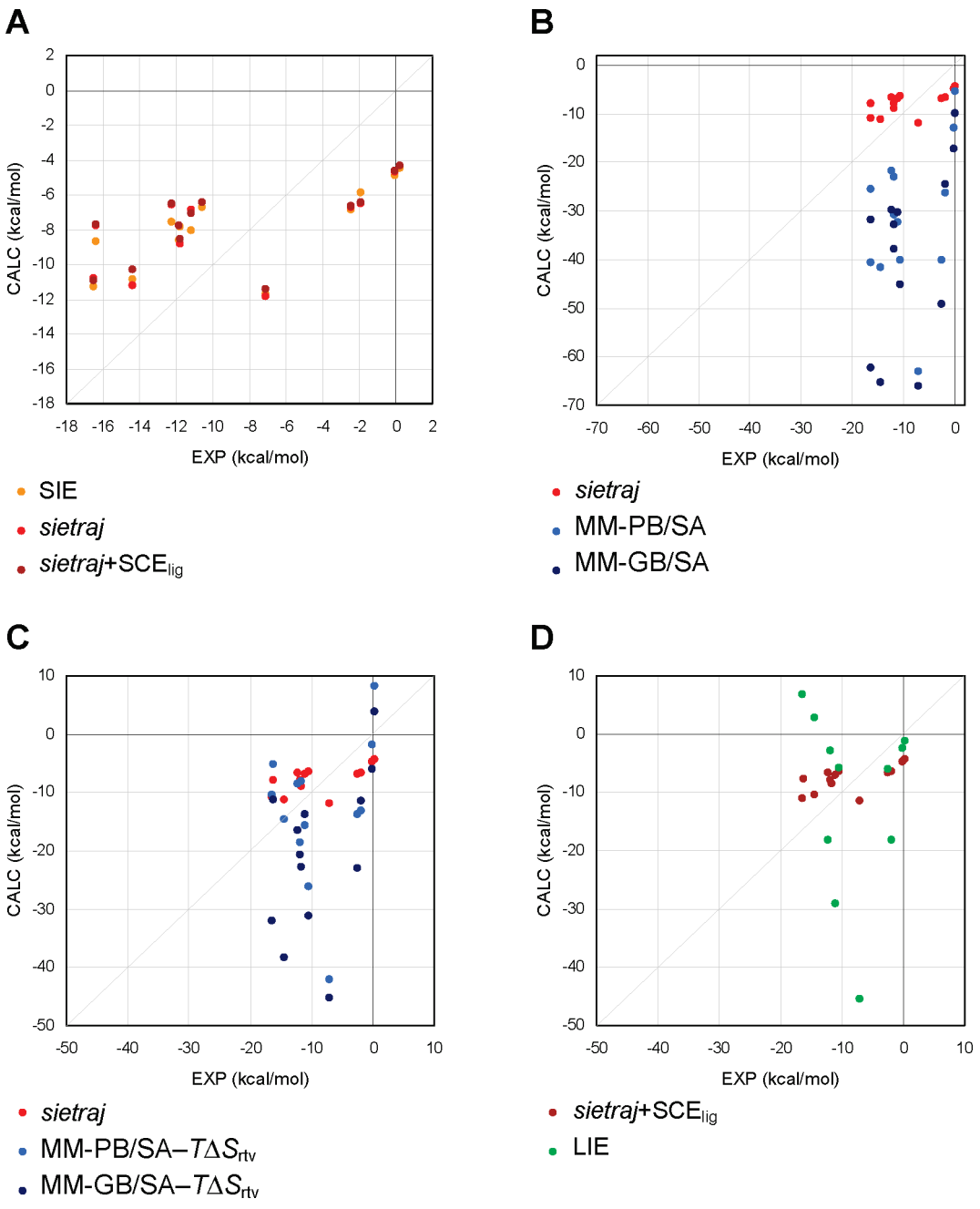

Figure 8. Molecular dynamics based predictions with several methods for a sample of SIE outliers. Five overestimated and 8 underestimated outliers by energy-minimized single-conformation-based SIE calculations were analyzed (with IDs, experimental data and prediction errors listed in Table 3). (A) Comparison of SIE predictions with those from the MD-based *sietraj* method without and with MD-averaged ligand strain contributions (SCE_{lig}). (B) Comparison of *sietraj* predictions with those from the MM-PB(GB)/SA methods. (B) Comparison of *sietraj* predictions with those from the MM-PB(GB)/SA methods including rotation, translation, and vibration entropy changes upon binding ($-T\Delta S_{rtv}$). (D) Comparison of *sietraj* predictions including ligand strain contributions (SCE_{lig}) with those from the LIE method.

This includes MD-averaged interaction energies with the explicit solvent, using published scaling coefficients for the van der Waals and Coulombic terms and including a continuum correction of long-range electrostatics (eq 5). The two-trajectory LIE method is similar in spirit with the *sietraj* plus the solvated ligand strain (SCE_{ligand}) discussed earlier. Again, while a few SIE outliers were partially corrected, others were significantly worsened, with overall errors and correlations below those of various implementations of the standard SIE function (Figure 8D, Table 3).

DISCUSSION

The SIE performance on the CSAR-NRC-HiQ data set of about 2 kcal/mol MUE in predicting absolute binding affinities is reasonable in light of the accuracy of the underlying continuum solvation model, which achieves MUEs between predicted and observed hydration free energies of small molecules in the 1.5−1.8 kcal/mol range, as tested prospectively in SAMPL experiments.[63,64] We cannot expect or believe that, in general, protein−ligand absolute binding affinity calculations, which

dx.doi.org/10.1021/ci2000242 |J. Chem. Inf. Model. 2011, 51, 2066–2081

Table 3. Molecular Dynamics Based Analysis of a Sample of SIE Outliers

		prediction errors[a]							
ID	ΔG_{exp}[a]	SIE	*sietraj*	*sietraj* +SCE_{lig}	MM-PB/SA	MM-GB/SA	MM-PB/SA−$T\Delta S_{rtv}$	MM-GB/SA−$T\Delta S_{rtv}$	LIE
					Overestimated Complexes				
1-96	−0.07	−4.79	**−4.63**[b]	**−4.53**	−12.88	−17.00	**−1.72**	−5.84	**−2.28**
1-104	0.21	−4.66	**−4.55**	**−4.52**	−5.57	−10.08	8.14	**3.63**	**−1.34**
2-127	−2.48	−4.39	**−4.23**	**−4.16**	−37.58	−46.70	−11.28	−20.40	**−3.48**
2-74	−7.11	−4.55	−4.74	**−4.31**	−55.77	−58.90	−34.99	−38.12	−38.37
2-184	−1.91	−3.92	−4.60	−4.51	−24.34	−22.49	−11.25	−9.40	−16.29
					Underestimated Complexes				
1-208	−11.12	3.12	4.32	4.12	−20.95	−19.12	−4.32	**−2.49**	−17.75
2-53	−11.87	3.25	4.09	4.13	−18.80	−20.97	−6.66	−8.83	9.02
2-269	−12.28	4.73	5.70	5.80	−9.38	−17.41	**3.88**	**−4.15**	−5.81
1-161	−14.42	3.58	**3.25**	4.12	−27.17	−50.86	**−0.09**	−23.78	17.33
1-173	−10.63	3.93	4.21	4.21	−29.39	−34.44	−15.53	−20.58	4.98
2-188	−16.51	5.27	5.73	5.63	−24.08	−45.70	6.18	−15.44	23.26
1-116	−16.37	7.70	8.63	8.66	−9.17	−15.32	11.34	**5.19**	37.30
1-168	−11.79	3.95	**2.98**	**3.24**	−11.25	−26.11	**3.83**	−11.03	37.20
MUE [a]		4.45	4.74	4.76	22.03	29.62	9.17	12.99	16.49
R^2		0.52	0.37	0.40	0.12	0.25	0.04	0.23	0.10

[a] In kcal/mol. [b] Prediction errors in bold are smaller in absolute value than those obtained with the single-conformation SIE method.

require predictions for solute−solute interactions as well as solvation of protein-size molecular systems, can be done with lower errors than those for small-molecule hydration free energy predictions.

Careful curation of the CSAR data set in terms of protonation and tautomeric states in the ligand-binding site region, resulting in the CSAR-NRC-HiQ version, was critical for a meaningful evaluation of the SIE performance. Relative to an earlier version of the CSAR data set, approximately 13% of ligands and 20% of proteins were affected by changes in protonation and tautomerism. The effect on standard SIE performance was large: 144 kcal/mol reduction of the cumulative absolute error (Table 2), 0.42 and 0.62 kcal/mol reductions in the overall MUE and RMSE, respectively, and R^2 increase from 0.19 to 0.38 and ρ_S from 0.47 to 0.62 (Table 1). Included in these improvements was the assignment of metal ions with the ligand rather than as part of the protein (the usual procedure) in a small fraction of complexes (3%) with metal ions bound loosely to protein atoms but interacting strongly with negatively charged ligands. It will be of interest to find out whether a more advanced curation of protonation and tautomerism, based on separate thermodynamic calculations in the bound state and in the free state, can further improve predictions.

The significant effects of protonation/tautomerism changes, of different assignments of bridging metal ions to the protein or ligand depending on topology, and even of single proton reorientation, illustrate a general sensitivity of force field−based scoring functions to atomic details. If the underlying structure and chemistry are not correctly represented, then first-principle scoring functions are bound to perform more poorly than empirical and knowledge-based scoring functions. This will be further accentuated on a data set like CSAR, which is highly diverse with respect to both proteins and ligands, and includes only a few series of congeneric ligands binding to the same protein or protein class, so there is minimal opportunity for error cancellation.

It has been noted that the SIE function extracts most of its signal from the nonpolar terms. The small improvement afforded by electrostatics to correlation with binding affinities aligns with the growing consensus that binding affinity is driven by nonpolar interactions, and electrostatic interactions, with a fine balance between its competing interactions and desolvation components, are required for introducing specificity to molecular recognition.[65] However, the electrostatic signal may become more important and even dominant if SIE is applied not only to active ligands with known binding modes as in the CSAR data set but also challenged with decoy poses of binders and decoy ligands. Preliminary tests on virtual screening enrichments point in this direction,[5] with more extensive VS enrichment tests needed.

An interesting idea for future development is to recalibrate the SIE function specifically for VS application against a combined data set including binding affinities for active ligands along with a set of suitably docked decoys that have a high probability of being inactive. This will retain a reasonable resolution in affinity prediction ability for binders and add classification power between binders and nonbinders. Additional energy terms can be incorporated, like an explicit hydrogen bonding term that may turn out quite useful in the VS mode of SIE. Moreover, the net advantage of *sietraj* consisting of MD-averaged SIE values versus single-conformation SIE predictions may become apparent for filtering out VS false-positive hits. The strain and entropic terms based on MD ensembles can be included but will have to be properly calibrated in a self-consistent manner within the SIE function and with inclusion of inactive decoys.

The current data on improving SIE outliers from the CSAR data set did not show an advantage of *sietraj*, as well as inclusion of ligand strain and explicit entropy contributions based on MD simulations. Various tests were carried out on a sample of outliers from single energy-minimized-conformation SIE calculations. MD-based *sietraj*, ligand strain, and applications of other physics-based methods

like MM-PB(GB)/SA without and with entropy estimates, and LIE, were unable to correct the predictions. This indicates a need for either incremental improvement in many areas of the molecular mechanics formalism (e.g., force-field, solvation model, electrostatic model) or a need for a paradigm shift in order to make a significant leap in prediction performance.

CONCLUSIONS

The Community Structure−Activity Resource distributed a first data set of 343 protein−ligand complexes that is diverse in both protein and ligand space. This constituted an excellent opportunity to benchmark the target-generic SIE function for predicting absolute binding affinities. The focus was on testing the single-conformation application mode of SIE, based on restrained energy-minimized crystal structures. Preparation of the data set in terms of protonation and tautomeric states at the protein−ligand interface was critical in order to evaluate the SIE performance. In curating these states, 13% of ligands and 20% of proteins were affected relative to an earlier version based on automatic preparation, leading to a substantial improvement in SIE performance. Proton orientation beyond that provided by energy minimization had a negligible overall effect, while underscoring the sensitivity of the SIE function to atomic details in specific cases. Also, assignment of interface metal ions to the ligand rather than to protein (as done usually) when the ion is loosely bound to protein but tightly bound to ligand (3% of complexes) was critical to accurate SIE predictions for such complexes. We believe that the performance of the SIE function, with a mean-unsigned-error slightly below 2 kcal/mol, lives up to expectations in light of the accuracy of underlying solvation models. Reparametrization on the curated CSAR-NRC-HiQ data set led to marginal improvements in performance and minimal changes in the optimal set of physical parameters; therefore, it does not seem warranted at this time. We find that the binding electrostatics contributes marginally to the performance of SIE function, in line with the current view that binding affinity is driven mainly by nonpolar interactions. Tests using MD-ensemble averaging, including ligand strain, applying different implementations of the end-point solvated interaction formalism, or treating the solvent explicitly did not improve further the outliers from the single-conformation SIE predictions.

ASSOCIATED CONTENT

Supporting Information. Minimal manual curation on the CSAR-HiQ preparation (Table S1), metal ion parameters (Table S2), ligand protonation changes (Table S3), protein protonation changes (Table S4), SIE physical parameters refitted on the two halves of the CSAR data set (Table S5), listing of complexes with polar H orientation changes beyond those from energy minimization (Table S6), complexes with metal ion assigned to ligand (Table S7), listing of experimental binding affinities and SIE with its component terms calculated on the CSAR-NRC-HiQ preparation (Table S8), past performance of the standard SIE function on various data sets (Figure S1), additional examples for changes between the CSAR-HiQ to CSAR-NRC-HiQ preparations (Figure S2), overall improvement of SIE predictions from the CSAR-HiQ preparation to the CSAR-NRC-HiQ preparation (Figure S3), and correlations with the ligand molecular weight for SIE and experimental values (Figure S4). This material is available free of charge via the Internet at http://pubs.acs.org.

AUTHOR INFORMATION

Corresponding Author

*Phone: (514)-496-1924. Fax: (514)-496-5143. E-mail: traian.sulea@nrc-cnrc.gc.ca.

ACKNOWLEDGMENT

We thank Hervé Hogues and Christopher Corbeil for useful discussions. This is NRC Canada publication number 53149.

REFERENCES

(1) Ferrara, P.; Gohlke, H.; Price, D. J.; Klebe, G.; Brooks, C. L. Assessing Scoring Functions for Protein-Ligand Interactions. *J. Med. Chem.* **2004**, *47*, 3032–3047.

(2) Wang, R.; Lu, Y.; Fang, X.; Wang, S. An Extensive Test of 14 Scoring Functions Using the PDBbind Refined Set of 800 Protein-Ligand Complexes. *J. Chem. Inf. Comput. Sci.* **2004**, *44*, 2114–2125.

(3) Warren, G. L.; Andrews, C. W.; Capelli, A. M.; Clarke, B.; LaLonde, J.; Lambert, M. H.; Lindvall, M.; Nevins, N.; Semus, S. F.; Senger, S.; Tedesco, G.; Wall, I. D.; Woolven, J. M.; Peishoff, C. E.; Head, M. S. A Critical Assessment of Docking Programs and Scoring Functions. *J. Med. Chem.* **2006**, *49*, 5912–5931.

(4) Gohlke, H.; Klebe, G. Approaches to the Description and Prediction of the Binding Affinity of Small-Molecule Ligands to Macromolecular Receptors. *Angew. Chem., Int. Ed.* **2002**, *41*, 2644–2676.

(5) Naim, M.; Bhat, S.; Rankin, K. N.; Dennis, S.; Chowdhury, S. F.; Siddiqi, I.; Drabik, P.; Sulea, T.; Bayly, C. I.; Jakalian, A.; Purisima, E. O. Solvated Interaction Energy (SIE) for Scoring Protein-Ligand Binding Affinities. 1. Exploring the Parameter Space. *J. Chem. Inf. Model.* **2007**, *47*, 122–133.

(6) Cui, Q.; Sulea, T.; Schrag, J. D.; Munger, C.; Hung, M. N.; Naim, M.; Cygler, M.; Purisima, E. O. Molecular Dynamics-Solvated Interaction Energy Studies of Protein-Protein Interactions: The MP1-p14 Scaffolding Complex. *J. Mol. Biol.* **2008**, *379*, 787–802.

(7) Kollman, P. A.; Massova, I.; Reyes, C.; Kuhn, B.; Huo, S.; Chong, L.; Lee, M.; Lee, T.; Duan, Y.; Wang, W.; Donini, O.; Cieplak, P.; Srinivasan, J.; Case, D. A.; Cheatham, T. E. Calculating Structures and Free Energies of Complex Molecules: Combining Molecular Mechanics and Continuum Models. *Acc. Chem. Res.* **2000**, *33*, 889–897.

(8) Kuhn, B.; Gerber, P.; Schulz-Gasch, T.; Stahl, M. Validation and Use of the MM-PBSA Approach for Drug Discovery. *J. Med. Chem.* **2005**, *48*, 4040–4048.

(9) Gohlke, H.; Kiel, C.; Case, D. A. Converging free energy estimates: MM-PB(GB)SA studies on the protein-protein complex Ras-Raf. *J. Comput. Chem.* **2004**, *25*, 238–250.

(10) Aqvist, J.; Marelius, J. The linear interaction energy method for predicting ligand binding free energies. *Comb. Chem. High Throughput Screening* **2001**, *4*, 613–626.

(11) Aqvist, J.; Luzhkov, V. B.; Brandsdal, B. O. Ligand Binding Affinities from MD Simulations. *Acc. Chem. Res.* **2002**, *35*, 358–365.

(12) Rankin, K. N.; Sulea, T.; Purisima, E. O. On the transferability of hydration-parametrized continuum electrostatics models to solvated binding calculations. *J. Comput. Chem.* **2003**, *25*, 954–962.

(13) Chen, W.; Chang, C. E.; Gilson, M. K. Calculation of Cyclodextrin Binding Affinities: Energy, Entropy, and Implications for Drug Design. *Biophys. J.* **2004**, *87*, 3035–3049.

(14) Chang, C. E.; Gilson, M. K. Free Energy, Entropy, and Induced Fit in Host−Guest Recognition: Calculations with the Second-Generation Mining Minima Algorithm. *J. Am. Chem. Soc.* **2004**, *126*, 13156–13164.

(15) Sulea, T.; Purisima, E. O. The solvated interaction energy (SIE) method for scoring binding affinities. In *Methods in Molecular Biology, Computer-Aided Drug Design*; Baron, R., Ed.; Humana Press: USA (Springer publishing group): 2011, submitted for publication.

(16) Guthrie, J. P. A Blind Challenge for Computational Solvation Free Energies: Introduction and Overview. *J. Phys. Chem. B* **2009**, *113*, 4501–4507.

(17) Geballe, M.; Skillman, A.; Nicholls, A.; Guthrie, J.; Taylor, P. The SAMPL2 blind prediction challenge: introduction and overview. *J. Comput.-Aided Mol. Des.* **2010**, *24*, 259–279.
(18) Skillman, A.; Geballe, M.; Nicholls, A. SAMPL2 challenge: prediction of solvation energies and tautomer ratios. *J. Comput.-Aided Mol. Des.* **2010**, *24* (4), 257–258.
(19) Skillman, G. SAMPL1 at first glance. *CUP-IX Meeting*, Santa Fe, NM, March 19, 2008, http://eyesopen.com/2008_cup_presentations/CUP9_Skillman.pdf (accessed July 11, 2011).
(20) Wang, Y. T.; Su, Z. Y.; Hsieh, C. H.; Chen, C. L. Predictions of Binding for Dopamine D2 Receptor Antagonists by the SIE Method. *J. Chem. Inf. Model.* **2009**, *49*, 2369–2375.
(21) Mishra, N. K.; Kriz, Z.; Wimmerova, M.; Koca, J. Recognition of selected monosaccharides by Pseudomonas aeruginosa Lectin II analyzed by molecular dynamics and free energy calculations. *Carbohydr. Res.* **2010**, *345*, 1432–1441.
(22) Rodriguez-Granillo, A.; Sedlak, E.; Wittung-Stafshede, P. Stability and ATP Binding of the Nucleotide-binding Domain of the Wilson Disease Protein: Effect of the Common H1069Q Mutation. *J. Mol. Biol.* **2008**, *383*, 1097–1111.
(23) Wei, C.; Mei, Y.; Zhang, D. Theoretical study on the HIV-1 integrase-5CITEP complex based on polarized force fields. *Chem. Phys. Lett.* **2010**, *495*, 121–124.
(24) Lecaille, F.; Chowdhury, S.; Purisima, E.; Bromme, D.; Lalmanach, G. The S2 subsites of cathepsins K and L and their contribution to collagen degradation. *Protein Sci.* **2007**, *16*, 662–670.
(25) Nguyen, M.; Marcellus, R. C.; Roulston, A.; Watson, M.; Serfass, L.; Murthy Madiraju, S. R.; Goulet, D.; Viallet, J.; Belec, L.; Billot, X.; Acoca, S.; Purisima, E.; Wiegmans, A.; Cluse, L.; Johnstone, R. W.; Beauparlant, P.; Shore, G. C. Small molecule obatoclax (GX15−070) antagonizes MCL-1 and overcomes MCL-1-mediated resistance to apoptosis. *Proc. Natl. Acad. Sci. U.S.A.* **2007**, *104*, 19512–19517.
(26) Okamoto, M.; Takayama, K.; Shimizu, T.; Muroya, A.; Furuya, T. Structure-activity relationship of novel DAPK inhibitors identified by structure-based virtual screening. *Bioorg. Med. Chem.* **2010**, *18*, 2728–2734.
(27) Yang, B.; Hamza, A.; Chen, G.; Wang, Y.; Zhan, C. G. Computational Determination of Binding Structures and Free Energies of Phosphodiesterase-2 with Benzo[1,4]diazepin-2-one Derivatives. *J. Phys. Chem. B* **2010**, *114*, 16020–16028.
(28) Wimmerova, M.; Mishra, N.; Pokorna, M.; Koca, J. Importance of oligomerisation on Pseudomonas aeruginosa Lectin-II binding affinity. In silico and in vitro mutagenesis. *J. Mol. Model.* **2009**, *15*, 673–679.
(29) Cornell, W. D.; Cieplak, P.; Bayly, C. I.; Gould, I. R.; Merz, K. M.; Ferguson, D. M.; Spellmeyer, D. C.; Fox, T.; Caldwell, J. W.; Kollman, P. A. A Second Generation Force Field for the Simulation of Proteins, Nucleic Acids, and Organic Molecules. *J. Am. Chem. Soc.* **1995**, *117*, 5179–5197.
(30) Bayly, C. I.; Cieplak, P.; Cornell, W. D.; Kollman, P. A. A well-behaved electrostatic potential based method using charge restraints for deriving atomic charges: The RESP model. *J. Phys. Chem.* **1993**, *97*, 10269–10280.
(31) Cornell, W. D.; Cieplak, P.; Bayly, C. I.; Kollman, P. A. Application of RESP charges to calculate conformational energies, hydrogen bond energies, and free energies of solvation. *J. Am. Chem. Soc.* **1993**, *115*, 9620–9631.
(32) Jakalian, A.; Bush, B. L.; Jack, D. B.; Bayly, C. I. Fast, efficient generation of high-quality atomic charges. AM1-BCC model: I. Method. *J. Comput. Chem.* **2000**, *21*, 132–146.
(33) Jakalian, A.; Jack, D. B.; Bayly, C. I. Fast, efficient generation of high-quality atomic charges. AM1-BCC model: II. Parameterization and validation. *J. Comput. Chem.* **2002**, *23*, 1623–1641.
(34) Wang, J.; Wang, W.; Kollman, P. A.; Case, D. A. Automatic atom type and bond type perception in molecular mechanical calculations. *J. Mol. Graphics Modell.* **2006**, *25*, 247–260.
(35) Wang, J.; Wolf, R. M.; Caldwell, J. W.; Kollman, P. A.; Case, D. A. Development and testing of a general amber force field. *J. Comput. Chem.* **2004**, *25*, 1157–1174.
(36) Case, D. A.; Cheatham, T. E.; Darden, T.; Gohlke, H.; Luo, R.; Merz, K. M.; Onufriev, A.; Simmerling, C.; Wang, B.; Woods, R. J. The Amber biomolecular simulation programs. *J. Comput. Chem.* **2005**, *26*, 1668–1688.
(37) Purisima, E. O.; Nilar, S. H. A Simple yet Accurate Boundary Element Method for Continuum Dielectric Calculations. *J. Comput. Chem.* **1995**, *16*, 681–689.
(38) Purisima, E. O. Fast summation boundary element method for calculating solvation free energies of macromolecules. *J. Comput. Chem.* **1998**, *19*, 1494–1504.
(39) Chan, S. L.; Purisima, E. O. A new tetrahedral tesselation scheme for isosurface generation. *Comput. Graphics* **1998**, *22*, 83–90.
(40) Chan, S. L.; Purisima, E. O. Molecular surface generation using marching tetrahedra. *J. Comput. Chem.* **1998**, *19*, 1268–1277.
(41) Bhat, S.; Purisima, E. O. Molecular surface generation using a variable-radius solvent probe. *Proteins* **2006**, *62*, 244–261.
(42) Case, D. A; Darden, T. A.; Cheatham, T. E., III; Simmerling, C. L.; Wang, J.; Duke, R. E.; Luo, R.; Crowley, M.; Walker, R. C.; Zhang, W.; Merz, K. M.; Wang, B.; Hayik, S.; Roitberg, A.; Seabra, G.; Kolossvary, I.; Wong, K. F.; Paesani, F.; Vanicek, J.; Wu, X.; Brozell, S. R.; Steinbrecher, T.; Gohlke, H.; Yang, L.; Tan, C.; Mongan, J.; Hornak, V.; Cui, G.; Mathews, D. H.; Seetin, M. G.; Sagui, C.; Babin, V.; Kollman, P. A. *AMBER 10*; University of California: San Francisco, CA, 2008.
(43) Jorgensen, W. L.; Chandrasekhar, J.; Madura, J. D.; Impey, R. W.; Klein, M. L. Comparison of simple potential functions for simulating liquid water. *J. Chem. Phys.* **1983**, *79*, 926–935.
(44) Hornak, V.; Abel, R.; Okur, A.; Strockbine, B.; Roitberg, A.; Simmerling, C. Comparison of multiple Amber force fields and development of improved protein backbone parameters. *Proteins* **2006**, *65*, 712–725.
(45) Wang, J.; Cieplak, P.; Kollman, P. A. How well does a restrained electrostatic potential (RESP) model perform in calculating conformational energies of organic and biological molecules? *J. Comput. Chem.* **2000**, *21*, 1049–1074.
(46) Darden, T.; York, D.; Pedersen, L. Particle mesh Ewald: An N. log(N) method for Ewald sums in large systems. *J. Chem. Phys.* **1993**, *98*, 10089–10092.
(47) Ryckaert, J. P.; Ciccotti, G.; Berendsen, H. J. C. Numerical integration of the cartesian equations of motion of a system with constraints: molecular dynamics of n-alkanes. *J. Comput. Phys.* **1977**, *23*, 327–341.
(48) Onufriev, A.; Bashford, D.; Case, D. A. Modification of the Generalized Born Model Suitable for Macromolecules. *J. Phys. Chem. B* **2000**, *104*, 3712–3720.
(49) Honig, B.; Sharp, K.; Yang, A. S. Macroscopic models of aqueous solutions: biological and chemical applications. *J. Phys. Chem.* **1993**, *97*, 1101–1109.
(50) Sitkoff, D.; Sharp, K. A.; Honig, B. Accurate Calculation of Hydration Free Energies Using Macroscopic Solvent Models. *J. Phys. Chem.* **1994**, *98*, 1978–1988.
(51) McQuarrie, D. A. *Statistical Mechanics*; Harper & Row: New York, NY, 1976.
(52) Aqvist, J.; Medina, C.; Samuelsson, J. E. A new method for predicting binding affinity in computer-aided drug design. *Protein Eng.* **1994**, *7*, 385–391.
(53) Lee, F. S.; Chu, Z. T.; Bolger, M. B.; Warshel, A. Calculations of antibody-antigen interactions: microscopic and semi-microscopic evaluation of the free energies of binding of phosphorylcholine analogs to McPC603. *Protein Eng.* **1992**, *5*, 215–228.
(54) Almlof, M.; Carlsson, J.; Aqvist, J. Improving the Accuracy of the Linear Interaction Energy Method for Solvation Free Energies. *J. Chem. Theory Comput.* **2007**, *3*, 2162–2175.
(55) Sulea, T.; Corbeil, C. R.; Purisima, E. O. Rapid Prediction of Solvation Free Energy. 1. An Extensive Test of Linear Interaction Energy (LIE). *J. Chem. Theory Comput.* **2010**, *6*, 1608–1621.
(56) Liljas, A.; Hakansson, K.; Jonsson, B. H.; Xue, Y. Inhibition and catalysis of carbonic anhydrase. Recent crystallographic analyses. *Eur. J. Biochem.* **1994**, *219*, 1–10.

(57) Weber, A.; Casini, A.; Heine, A.; Kuhn, D.; Supuran, C. T.; Scozzafava, A.; Klebe, G. Unexpected nanomolar inhibition of carbonic anhydrase by COX-2-selective celecoxib: new pharmacological opportunities due to related binding site recognition. *J. Med. Chem.* **2004**, *47*, 550–557.

(58) Trylska, J.; Antosiewicz, J.; Geller, M.; Hodge, C. N.; Klabe, R. M.; Head, M. S.; Gilson, M. K. Thermodynamic linkage between the binding of protons and inhibitors to HIV-1 protease. *Protein Sci.* **1999**, *8*, 180–195.

(59) Czodrowski, P.; Sotriffer, C. A.; Klebe, G. Atypical Protonation States in the Active Site of HIV-1 Protease: A Computational Study. *J. Chem. Inf. Model.* **2007**, *47*, 1590–1598.

(60) Harte, W. E.; Beveridge, D. L. Prediction of the protonation state of the active site aspartyl residues in HIV-1 protease-inhibitor complexes via molecular dynamics simulation. *J. Am. Chem. Soc.* **1993**, *115*, 3883–3886.

(61) Barford, D.; Flint, A. J.; Tonks, N. K. Crystal structure of human protein tyrosine phosphatase 1B. *Science* **1994**, *263*, 1397–1404.

(62) Dillet, V.; Van Etten, R. L.; Bashford, D. Stabilization of Charges and Protonation States in the Active Site of the Protein Tyrosine Phosphatases: A Computational Study. *J. Phys. Chem. B* **2000**, *104*, 11321–11333.

(63) Sulea, T.; Wanapun, D.; Dennis, S.; Purisima, E. O. Prediction of SAMPL-1 Hydration Free Energies Using a Continuum Electrostatics-Dispersion Model. *J. Phys. Chem. B* **2009**, *113*, 4511–4520.

(64) Purisima, E.; Corbeil, C.; Sulea, T. Rapid prediction of solvation free energy. 3. Application to the SAMPL2 challenge. *J. Comput.-Aided Mol. Des.* **2010**, *24*, 373–383.

(65) Sulea, T.; Purisima, E. O. Profiling charge complementarity and selectivity for binding at the protein surface. *Biophys. J.* **2003**, *84*, 2883–2896.